Unsteady Aerodynamic Modeling and Longitudinal Adaptive Tracking Control for Hypersonic Vehicles with Sweep Variation

Yanqi Feng, Zhigang Wu and Haizhao Liang*

School of Aeronautics and Astronautics, Sun Yat-Sen University, Shenzhen, 510275, China

Abstract: This paper investigates the longitudinal control problem of a sweep-varying hypersonic vehicle in the presence of unsteady aerodynamic effects, aerodynamic uncertainty, and actuator constraints. In contrast to existing adaptive or reinforcement-learning-based control methods that mainly treat sweep motion as a scheduling variable, the present study develops a unified control framework in which the sweep angle is exploited as an active control input and its nonstationary aerodynamic influence is explicitly incorporated into both aerodynamic modeling and controller design. First, a control-oriented unsteady aerodynamic model is established using the stochastic hierarchical Kriging (SHK) method, and its fidelity is quantitatively evaluated against high-fidelity aerodynamic data through drag-, lift-, and pitching-moment prediction errors. A constrained sweep-angle command and elevator command are then designed to satisfy actuator magnitude and rate limits while preserving longitudinal control effectiveness. To further improve transient performance under uncertain unsteady aerodynamics, an actor–critic reinforcement-learning module is embedded as a lightweight supervisory tuning layer on top of the adaptive controller, so that online policy improvement is achieved without repeated trial-and-error exploration. An observer-assisted implementation is also introduced to relax the full-state measurement requirement. Lyapunov analysis proves the boundedness of the closed-loop signals and establishes the stability of the observer–controller–learning interconnection. Numerical results from nominal ascent/descent tracking, disturbance rejection, RL-ablation comparison, and Monte Carlo shooting simulations show that the proposed method improves aerodynamic prediction fidelity, reduces tracking error and settling time, and enhances robustness relative to baseline adaptive and PID schemes.

Keywords: Sweep-Variation Hypersonic Aircraft, Neural network, Adaptive Tracking control.

1. INTRODUCTION

To satisfy increasingly demanding performance requirements in high-speed flight, researchers have continually explored advanced aerodynamic configurations and control strategies for next-generation aircraft. Inspired by birds' ability to adapt wing shape and flight posture to changing flight conditions, morphing aircraft have attracted sustained interest in the aerospace community. As a representative class of morphing vehicles, sweep-varying aircraft can adjust the wing sweep angle in response to mission demands and flight environments, thereby improving aerodynamic efficiency, maneuverability, and operational adaptability over a wide flight envelope [1, 9, 12, 13, 17]. In particular, sweep-varying hypersonic vehicles (SVHVs) introduce an additional configuration degree of freedom into the flight control system, creating new opportunities for lift-to-drag-ratio optimization, trajectory shaping, and integrated morphing-control design [27].

Compared with conventional fixed-configuration aircraft, morphing vehicles exhibit stronger aerodynamic nonlinearity, more significant parameter variations, and tighter coupling among aerodynamic characteristics, structural deformation, and flight dynamics. More importantly, their aerodynamic behavior is inherently unsteady during configuration transitions. When the wing sweep angle varies continuously, the aerodynamic forces and moments depend not only on the instantaneous flight state and configuration, but also on the deformation rate, transient flow evolution, and history-dependent aerodynamic effects. These unsteady aerodynamic characteristics are particularly important for hypersonic morphing vehicles, because even small configuration changes may cause substantial variations in aerodynamic coefficients and control effectiveness. Therefore, unsteady aerodynamic modeling is essential not only for aerodynamic analysis but also for controller design, stability assessment, and performance evaluation of morphing flight systems [1, 2, 3, 4, 21, 28, 37, 38].

Existing studies on morphing aircraft have mainly focused on configuration scheduling, coordinated control, and robust tracking under uncertainty. For example, gain-scheduled and linear-parameter-varying (LPV) approaches have been developed for morphing aircraft with varying aerodynamic configurations [7, 13]. Adaptive coordinated tracking, incremental sliding-mode control, prescribed-performance backstepping,

*Address correspondence to this author at the School of Aeronautics and Astronautics, Sun Yat-Sen University, Shenzhen, 510275, China;
E-mail: lianghch5@mail.sysu.edu.cn

Received on 09-04-2026 Accepted on 29-05-2026 Published on 09-06-2026

E-ISSN: 3083-3450/2026

and backstepping sliding-mode methods have also been applied to different morphing-aircraft platforms [12, 18, 17, 27]. In addition, neural-network-based adaptive control and dynamic-surface-control methods have been introduced to compensate for modeling uncertainty and input-output constraints in morphing aircraft [33, 34]. For hypersonic or air-breathing morphing vehicles, robust control, prescribed-time control, fixed-time control, and disturbance-observer-based sliding-mode control have shown promising performance in handling strong nonlinearity and disturbances [2, 4, 21, 37, 38]. Fault-tolerant and anti-disturbance control strategies have also been investigated for air-breathing hypersonic vehicles and flying-wing aircraft with actuator faults, state constraints, and immeasurable states [6, 16, 28]. Meanwhile, integrated guidance, control, and morphing design has been explored to improve the overall performance of hypersonic morphing vehicles during glide flight [1]. Although these studies have significantly advanced the control of morphing and hypersonic vehicles, most remain focused on configuration change, trajectory tracking, or robust stabilization, whereas the control problem associated with unsteady aerodynamic effects induced by continuous morphing remains insufficiently studied.

In addition to model-based control methods, learning-based approaches have gradually emerged as effective tools for handling nonlinear, uncertain, and time-varying systems. Classical adaptive neural control and composite learning frameworks have demonstrated strong approximation and compensation capabilities for uncertain nonlinear systems [8, 23, 35]. In aerospace applications, adaptive control with neural architectures, self-organizing model-reference adaptive control, and incremental-learning-based design have been investigated for aircraft, hypersonic vehicles, and spacecraft disturbance-rejection problems [3, 10, 25]. Moreover, near-optimal tracking and neural-network-based performance analysis have been developed for partially unknown nonlinear systems and aerospace mission scenarios [11, 15, 24, 32]. These developments suggest that data-driven or learning-assisted control can provide additional flexibility beyond conventional model-based methods, particularly when accurate analytical models are difficult to obtain.

Among these learning-based approaches, reinforcement learning (RL) has shown particular promise for control problems involving unknown dynamics, nonlinear coupling, and sequential decision-making. Existing studies have applied RL or Q-learning to morphing-aircraft shape decision, switch control, and autonomous morphing-strategy design [9, 14, 39]. Dueling-DQN has also been used for coordinated intelligent control of flight-control systems and shape variation in variable-sweep morphing aircraft [36]. More generally, RL-enhanced backstepping and optimal control methods have been developed for nonlinear strict-feedback systems, stochastic nonlinear systems, and multi-agent systems [20, 29, 30, 31, 40]. Related studies on value-function learning, Q-learning, and recurrent-neural-network-based RL have further demonstrated the capability of RL to address continuous-control and nonlinear optimal-control problems [19, 22, 26]. In addition, deep reinforcement learning has been introduced into switched-flight-vehicle tracking control, demonstrating its potential to improve robustness and control adaptability in aerospace systems [5]. Nevertheless, for sweep-varying hypersonic vehicles with pronounced unsteady aerodynamic effects, the application of RL to longitudinal control design remains limited. This limitation is particularly evident when the objective extends beyond configuration scheduling to the unified treatment of aerodynamic uncertainty, unsteady morphing effects, and command-tracking performance.

Motivated by the above considerations, this paper investigates the longitudinal control problem of a sweep-varying hypersonic vehicle under unsteady aerodynamic effects, actuator constraints, and model uncertainty. Different from studies that mainly regard sweep variation as a scheduling mechanism or consider only static aerodynamic-parameter changes, the present work explicitly treats sweep motion as an active control degree of freedom and incorporates the associated nonstationary aerodynamic influence into the control design process. Based on an SHK-based unsteady aerodynamic model, a control-oriented longitudinal dynamic formulation is established. On this basis, a constrained sweep-angle command and a reinforcement-learning-assisted control mechanism are integrated into a unified control framework for longitudinal command tracking and robustness enhancement.

Compared with existing adaptive backstepping or RL-assisted morphing-control studies, the novelty of this work lies in three aspects. First, the unsteady aerodynamic effect induced by sweep-rate-dependent morphing is not treated as an unmodeled residual but embedded into a validated SHK-based control-oriented formulation with an explicitly identified lag state. Second, instead of using the sweep angle merely as a

geometric scheduler, a dedicated constrained sweep-angle command is designed so that morphing action directly participates in longitudinal force/moment regulation under magnitude and rate limits. Third, the reinforcement-learning module is not used as a stand-alone black-box controller; rather, it acts as an actor–critic supervisory tuner integrated with the adaptive controller, thereby preserving Lyapunov-based stability while improving transient performance.

The main contributions of this paper are summarized as follows. First, an SHK-based unsteady aerodynamic model is incorporated into a control-oriented longitudinal formulation, in which the delayed aerodynamic effect induced by sweep motion is explicitly represented through a lag-state description. Second, a dedicated sweep-angle command is designed under actuator amplitude and rate constraints, so that the sweep angle participates in control as an active constrained input rather than a passive scheduling parameter. Third, a Critic-Actor reinforcement-learning module is introduced as a lightweight supervisory tuner to improve transient performance and adaptability under uncertain unsteady aerodynamic conditions. Fourth, the boundedness of the closed-loop system is established through Lyapunov analysis, and the effectiveness and robustness of the proposed method are validated through ascent-profile simulations and Monte Carlo shooting tests.

2. UNSTEADY AERODYNAMIC MODELING AND CONTROL-ORIENTED AERODYNAMIC FORMULATION

2.1. Unsteady Aerodynamic Modeling of the Sweep-Varying Vehicle

To describe the aerodynamic characteristics of the sweep-varying hypersonic vehicle during continuous morphing, an unsteady aerodynamic model is established for the longitudinal channel. Different from conventional quasi-steady treatments, the present modeling framework explicitly accounts for the transient aerodynamic response induced by sweep motion. Such a formulation is necessary because, for a sweep-varying configuration, the aerodynamic loads are affected not only by the instantaneous flight state and geometric configuration, but also by the morphing rate and the associated unsteady flow evolution.

The vehicle is considered over a wide flight envelope with representative sweep-angle configurations covering the major morphing states. In the modeling process, the sweep motion is treated as a prescribed time-dependent kinematic input, such that the aerodynamic effects induced by configuration variation can be explicitly identified. Under this formulation, the sweep angle is represented as a function of time, and the sweep rate directly characterizes the temporal variation of the aerodynamic loads. As a result, the longitudinal aerodynamic behavior during sweep transition can be described in a manner suitable for subsequent dynamic analysis and controller development.

Based on high-fidelity aerodynamic data, a reduced-order unsteady aerodynamic surrogate model is constructed using the stochastic hierarchical Kriging (SHK) framework. The purpose of introducing SHK is to establish an efficient mapping from flight states and morphing variables to aerodynamic coefficients while retaining the dominant nonlinear and time-dependent aerodynamic characteristics. Relative to repeated high-fidelity numerical simulations, this approach significantly improves computational efficiency and provides a compact aerodynamic representation for control-oriented applications.

For the longitudinal motion considered in this paper, the lift, drag, and pitching-moment coefficients are described as functions of the angle of attack, sweep angle, elevator deflection, Mach number, and sweep rate, namely

$$C_L = C_L(\alpha,\delta_h,\delta_e,Ma,\omega), \tag{1}$$

$$C_D = C_D(\alpha,\delta_h,\delta_e,Ma,\omega), \tag{2}$$

$$C_M = C_M(\alpha,\delta_h,\delta_e,Ma,\omega), \tag{3}$$

where α is the angle of attack, δ_h is the sweep angle, δ_e is the elevator deflection, Ma is the Mach number, and $\omega = \dot{\delta}_h$ denotes the sweep rate. The explicit dependence on ω distinguishes the present model from quasi-steady aerodynamic formulations and enables the non-stationary effect of sweep motion to be incorporated into the longitudinal dynamics.

Accordingly, the aerodynamic lift, drag, and pitching moment are written as

$$L = \bar{q}SC_L(\alpha,\delta_h,\delta_e,Ma,\omega), \tag{4}$$

$$D = \bar{q}SC_D(\alpha,\delta_h,\delta_e,Ma,\omega), \tag{5}$$

$$M = z_T T + \bar{q}S\bar{c}\,C_M(\alpha,\delta_h,\delta_e,Ma,\omega), \tag{6}$$

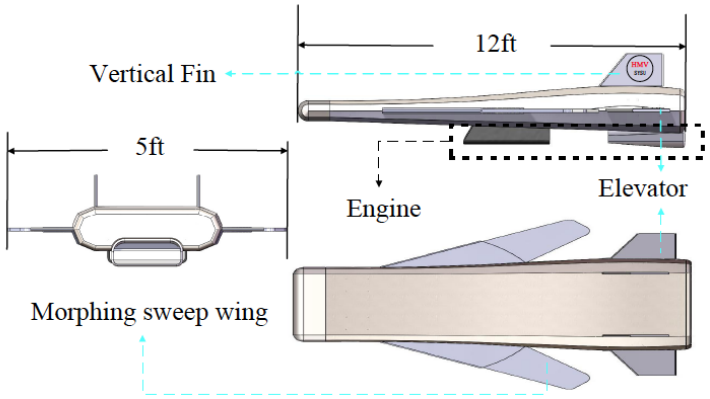

Figure 1: The sweep-varying vehicle.

where $\bar{q}$ is the dynamic pressure, S is the reference area, $\bar{c}$ is the mean aerodynamic chord, and z_T is the thrust moment arm. These expressions provide the aerodynamic basis for the control-oriented model constructed in the next subsection.

2.2. Control-Oriented Aerodynamic Formulation

The established unsteady aerodynamic model shows that the longitudinal aerodynamic characteristics are jointly determined by the instantaneous configuration and the morphing process itself. In particular, both sweep angle and sweep rate have a significant influence on the lift, drag, and pitching-moment responses. This implies that the aerodynamic behavior of the vehicle cannot be adequately represented by a purely static configuration-dependent model. Instead, the unsteady effect associated with continuous sweep motion must be retained in the control-oriented formulation.

From the aerodynamic perspective, the lift response exhibits an evident dependence on flight condition and sweep-motion state, indicating that sweep actuation contributes directly to longitudinal force generation rather than serving merely as a geometric scheduling variable. The drag response shows that different sweep configurations may lead to substantially different aerodynamic efficiency, especially in high-speed flight regimes, where sweep variation directly affects the energy characteristics of the vehicle. The pitching-moment response is even more critical for control design, because sweep variation modifies not only the moment magnitude but also the aerodynamic center location and the dynamic response of the longitudinal channel. These features demonstrate that a control-oriented aerodynamic model should explicitly reflect the transient effect of sweep motion on both force and moment generation.

To this end, the aerodynamic coefficients are decomposed into quasi-steady components and unsteady correction terms. The control-oriented aerodynamic formulation is written as

$$C_L = C_L^{qs}(\alpha,\delta_h,\delta_e,Ma) + \Delta C_L^u(\alpha,\delta_h,\delta_e,Ma,\omega), \tag{7}$$

$$C_D = C_D^{qs}(\alpha,\delta_h,\delta_e,Ma) + \Delta C_D^u(\alpha,\delta_h,\delta_e,Ma,\omega), \tag{8}$$

$$C_M = C_M^{qs}(\alpha,\delta_h,\delta_e,Ma) + \Delta C_M^u(\alpha,\delta_h,\delta_e,Ma,\omega,\xi_M), \tag{9}$$

where C_L^{qs}, C_D^{qs}, and C_M^{qs} denote the quasi-steady aerodynamic components, and ΔC_L^u, ΔC_D^u, and ΔC_M^u represent the unsteady corrections induced by sweep motion. The additional state ξ_M is introduced to characterize the aerodynamic memory effect in the pitching-moment response.

To preserve the delayed aerodynamic moment dynamics in a compact form, the lag state is described by

$$\dot{\xi}_M = -\frac{1}{\tau_M}\xi_M + \frac{1}{\tau_M}\Delta C_M^{SHK}(\alpha,\delta_h,\delta_e,Ma,\omega), \tag{10}$$

and the pitching-moment coefficient is rewritten as

$$C_M = C_M^{qs}(\alpha,\delta_h,\delta_e,Ma) + \xi_M, \tag{11}$$

where τ_M is the equivalent aerodynamic time constant and $\Delta C_M^{SHK}(\cdot)$ denotes the SHK-predicted unsteady pitching-moment increment. This representation retains the essential delayed response induced by sweep motion while remaining sufficiently compact for control analysis and synthesis.

By incorporating the above aerodynamic expressions into the longitudinal nonlinear dynamics, the control-oriented model is obtained as

$$\dot{V} = \frac{T\cos\alpha - D}{m} - g\sin\gamma + \frac{F_x\cos\alpha - F_y\sin\alpha}{m}, \tag{12}$$

$$\dot{h} = V\sin\gamma, \tag{13}$$

$$\dot{\gamma} = \frac{T\sin\alpha + L}{mV} - \frac{g\cos\gamma}{V} + \frac{F_x\sin\alpha + F_y\cos\alpha}{mV}, \tag{14}$$

$$\dot{\alpha} = Q - \dot{\gamma}, \tag{15}$$

$$\dot{Q} = \frac{M}{I_{yy}}, \tag{16}$$

together with the aerodynamic lag equation for ξ_M. The resulting control-oriented state vector is therefore given by

$$x = \begin{bmatrix} V & h & \gamma & \alpha & Q & \xi_M \end{bmatrix}^T, \tag{17}$$

with the control input defined as

$$u = \begin{bmatrix} \delta_h & \delta_e \end{bmatrix}^T. \tag{18}$$

The resulting formulation preserves the dominant non-stationary aerodynamic effects induced by sweep motion while avoiding the computational burden of repeated high-fidelity aerodynamic evaluation. More importantly, it establishes a direct dynamic interface between unsteady aerodynamic modeling and longitudinal control design, thereby providing the model basis for the adaptive tracking controller and subsequent learning-aided control enhancement developed in the following sections.

2.3. SHK Model Validation and Lag-State Identification

To verify the accuracy of the SHK-based unsteady aerodynamic model, the surrogate predictions are compared with high-fidelity aerodynamic data over representative operating conditions involving different sweep angles, sweep rates, and angles of attack. Quantitative validation metrics are introduced, including the mean absolute error (MAE), root-mean-square error (RMSE), and maximum absolute error (MaxAE), defined as

$$MAE = \frac{1}{N}\sum_{i=1}^{N}\left|y_i^{SHK} - y_i^{ref}\right|, \tag{19}$$

$$RMSE = \sqrt{\frac{1}{N}\sum_{i=1}^{N}\left(y_i^{SHK} - y_i^{ref}\right)^2}, \tag{20}$$

$$MaxAE = \max_{1\le i\le N}\left|y_i^{SHK} - y_i^{ref}\right|, \tag{21}$$

where y_i^{SHK} and y_i^{ref} denote the SHK prediction and the corresponding high-fidelity reference value, respectively.

The lag-state variable ξ_M introduced in the control-oriented aerodynamic formulation represents the delayed pitching-moment response caused by sweep-rate-dependent flow evolution. To identify the corresponding lag time constant τ_M, a first-order lag reconstruction is employed and the mismatch between the SHK-predicted unsteady pitching-moment increment and the lag-state reconstruction is minimized, i.e.,

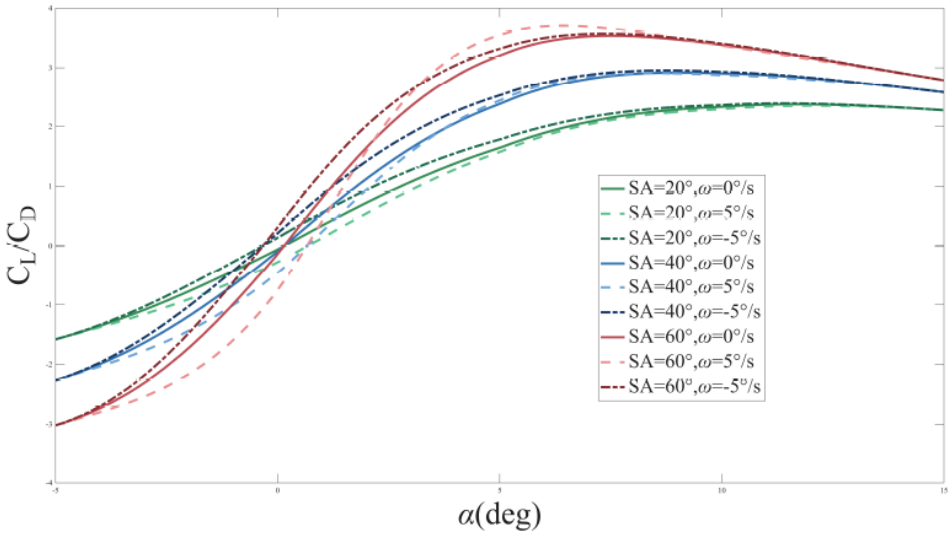

Figure 2: Representative variations of the longitudinal aerodynamic coefficients under different sweep angles and sweep rates.

Table 1: Quantitative Validation Metrics of the SHK-Based Unsteady Aerodynamic Model

Coefficient	MAE	RMSE	MaxAE
C_L	0.0128	0.0169	0.0415
C_D	0.0064	0.0087	0.0213
C_M	0.0086	0.0132	0.0338

$$\tau_M^* = \arg\min_{\tau_M>0} \sum_{i=1}^{N} \left[\xi_M^{rec}(t_i;\tau_M) - \Delta C_M^{SHK}(t_i) \right]^2, \tag{22}$$

where $\xi_M^{rec}(t_i;\tau_M)$ is the reconstructed lag response under a candidate τ_M. This identification process provides both a physical interpretation and a practical estimation procedure for the aerodynamic lag parameter.

Table **1** summarizes the quantitative validation results of the SHK model for the lift, drag, and pitching-moment coefficients. The results show that the proposed SHK formulation achieves sufficiently high prediction accuracy for control-oriented applications while preserving the dominant unsteady aerodynamic characteristics induced by sweep motion. These errors are computed over all validation samples across different sweep angles, sweep rates, and angles of attack.

3. ADAPTIVE TRACKING CONTROL DESIGN AND STABILITY ANALYSIS

3.1. Control Objective and Error Dynamics

Based on the control-oriented unsteady aerodynamic model established in Section 2, the longitudinal state vector is defined as

$$x = \begin{bmatrix} V & h & \gamma & \alpha & Q & \xi_M \end{bmatrix}^T, \tag{23}$$

where V, h, γ, α, Q, and ξ_M denote the velocity, altitude, flight-path angle, angle of attack, pitch rate, and aerodynamic lag state, respectively. The control input is chosen as

$$u = \begin{bmatrix} \delta_h & \delta_e \end{bmatrix}^T \tag{24}$$

where δ_h is the sweep angle and δ_e is the elevator deflection.

The control objective is to ensure that the velocity and altitude track their corresponding reference commands V_r and h_r in the presence of aerodynamic uncertainty, external disturbances, and sweep-induced unsteady aerodynamic effects. Since the altitude dynamics are mainly coupled with the flight-path angle, angle of attack, and pitch rate, the longitudinal control design is developed in a hierarchical manner. Specifically, the height-loop controller is constructed first, and the velocity-loop controller is then designed using a similar structure.

Define the tracking errors for the height loop as

$$e_h = h - h_r, \tag{25}$$

$$e_\gamma = \gamma - \gamma_r, \tag{26}$$

$$e_\alpha = \alpha - \alpha_r, \tag{27}$$

$$e_Q = Q - Q_r, \tag{28}$$

where γ_r, α_r, and Q_r are virtual control commands generated recursively.

To construct the outer-loop command, choose

$$\gamma_r = -k_h e_h + \dot{h}_r / V, \tag{29}$$

where $k_h > 0$ is a design parameter. Then the altitude tracking error dynamics satisfy

$$\dot{e}_h = V \sin\gamma - \dot{h}_r. \tag{30}$$

By linearization around the command trajectory and standard dynamic inversion arguments, the altitude loop can be transformed into a stabilizable structure in terms of e_h and e_γ.

3.2. Observer-Assisted State Reconstruction

The control design presented in this paper requires several longitudinal states, including the aerodynamic lag state ξ_M, which may not be directly measurable in practice. To relax the full-state-availability assumption, an observer-assisted implementation is introduced. Let the measurable output vector be denoted by

$$y = \begin{bmatrix} V & h & \gamma & \alpha & Q \end{bmatrix}^T, \tag{31}$$

and let $\hat{x}$ denote the estimated state vector. A compact extended-state-observer-type estimator is adopted in the form

$$\dot{\hat{x}} = f(\hat{x},u) + L_o(y - \hat{y}), \tag{32}$$

$$\hat{y} = C\hat{x}, \tag{33}$$

where L_o is the observer gain matrix. In particular, the aerodynamic lag state is reconstructed through the coupled pitch-channel dynamics and the SHK-based aerodynamic correction model.

Under appropriate observer gain selection, the estimation error remains bounded and converges to a small neighborhood of zero. Therefore, the controller can be implemented using the estimated states $\hat{x}$ instead of the true states x, while preserving the stability backbone of the adaptive control design. In the subsequent derivation, the nominal control law is first presented in terms of the true states for clarity, and its observer-assisted implementation follows directly by replacing unavailable states with their estimates.

3.3. Baseline Adaptive Control Design for the Height Loop

Considering the nonlinearity of the control-oriented aerodynamic model, the height loop is designed using an adaptive backstepping structure. The flight-path-angle dynamics can be written in the compact form

$$\dot{\gamma} = f_\gamma(x) + g_\gamma(x)\alpha + \Delta_\gamma(x,t), \tag{34}$$

where $f_\gamma(x)$ and $g_\gamma(x)$ denote known nominal nonlinear terms, and $\Delta_\gamma(x,t)$ collects the uncertain aerodynamic terms, unsteady corrections, lag-state effects, and external disturbances.

The virtual control command for the angle of attack is selected as

$$\alpha_r = -k_\gamma e_\gamma - \hat{\upsilon}_\gamma \Phi_\gamma(x) sat\left(\frac{e_\gamma}{\varepsilon_\gamma}\right) + \varphi_\gamma(x), \tag{35}$$

where $k_\gamma > 0$ is a feedback gain, $\hat{\upsilon}_\gamma$ is the adaptive estimate of the uncertainty bound, $\Phi_\gamma(x)$ is a known regression function, $\varepsilon_\gamma > 0$ is a small design constant, and $\varphi_\gamma(x)$ is the nominal compensation term.

Similarly, the angle-of-attack dynamics can be expressed as

$$\dot{\alpha} = f_\alpha(x) + g_\alpha(x)Q + \Delta_\alpha(x,t), \tag{36}$$

and the virtual pitch-rate command is designed as

$$Q_r = -k_\alpha e_\alpha - \hat{\upsilon}_\alpha \Phi_\alpha(x) sat\left(\frac{e_\alpha}{\varepsilon_\alpha}\right) + \varphi_\alpha(x), \tag{37}$$

where $k_\alpha > 0$, $\hat{\upsilon}_\alpha$, $\Phi_\alpha(x)$, ε_α, and $\varphi_\alpha(x)$ are defined analogously.

For the pitch-rate subsystem, the dynamics are written as

$$\dot{Q} = f_Q(x) + g_Q(x,\delta_h)\delta_e + \Delta_Q(x,t), \tag{38}$$

where the uncertainty term $\Delta_Q(x,t)$ includes the residual effects of the control-oriented unsteady pitching-moment model, especially the lag-state contribution ξ_M. The elevator control law is then designed as

$$\delta_e = g_Q^{-1}(x,\delta_h)\left[-k_Q e_Q - \hat{\upsilon}_Q \Phi_Q(x) sat\left(\frac{e_Q}{\varepsilon_Q}\right) + \dot{Q}_r - \varphi_Q(x)\right], \tag{39}$$

where $k_Q > 0$, $\hat{\upsilon}_Q$, $\Phi_Q(x)$, ε_Q, and $\varphi_Q(x)$ are design quantities.

In the present problem, the sweep angle δ_h is not merely a scheduling parameter but an active control input that affects both force and moment generation through the unsteady aerodynamic model. Therefore, the sweep-angle control law is designed to regulate the aerodynamic configuration and improve the transient longitudinal response. A compact sweep-angle command is chosen as

$$\delta_h = -k_s e_\gamma - k_{sh} e_h - \hat{\upsilon}_s \Phi_s(x) sat\left(\frac{e_\gamma}{\varepsilon_s}\right) + \varphi_s(x), \tag{40}$$

where $k_s > 0$, $k_{sh} > 0$, $\hat{\upsilon}_s$, $\Phi_s(x)$, ε_s, and $\varphi_s(x)$ are appropriately selected such that the sweep motion contributes to both aerodynamic-force regulation and configuration adaptation.

To simplify the adaptive design, the lumped uncertainty bound is introduced as

$$\upsilon_H = \upsilon_\gamma + \upsilon_\alpha + \upsilon_Q + \upsilon_s, \tag{41}$$

with the corresponding estimation error

$$\tilde{\upsilon}_H = \upsilon_H - \hat{\upsilon}_H. \tag{42}$$

The adaptive update law is selected as

$$\dot{\hat{\upsilon}}_H = \frac{1}{\tau_{H,3}}\left[e_\gamma \Phi_\gamma(x) sat\left(\frac{e_\gamma}{\varepsilon_\gamma}\right) + e_\alpha \Phi_\alpha(x) sat\left(\frac{e_\alpha}{\varepsilon_\alpha}\right) + e_Q \Phi_Q(x) sat\left(\frac{e_Q}{\varepsilon_Q}\right) + e_\gamma \Phi_s(x) sat\left(\frac{e_\gamma}{\varepsilon_s}\right) - \kappa_{H,3}\hat{\upsilon}_H \right]. \tag{43}$$

where $\tau_{H,3} > 0$ and $\kappa_{H,3} > 0$ are adaptation parameters.

3.4. Velocity-Loop Control Design

The velocity dynamics can be expressed as

$$\dot{V} = f_V(x) + g_V(x)T + \Delta_V(x,t), \tag{44}$$

where T is the thrust input, and $\Delta_V(x,t)$ includes aerodynamic uncertainty, unsteady drag effects, and external disturbances. Define the velocity tracking error as

$$e_V = V - V_r. \tag{45}$$

The velocity control law is selected as

$$T = g_V^{-1}(x)\left[-k_V e_V - \hat{\upsilon}_V \Phi_V(x) sat\left(\frac{e_V}{\varepsilon_V}\right) + \dot{V}_r - \varphi_V(x) \right], \tag{46}$$

where $k_V > 0$, $\hat{\upsilon}_V$, $\Phi_V(x)$, ε_V, and $\varphi_V(x)$ are design parameters. The update law for the velocity uncertainty bound is chosen as

$$\dot{\hat{\upsilon}}_V = \frac{1}{\tau_V}\left[e_V \Phi_V(x) sat\left(\frac{e_V}{\varepsilon_V}\right) - \kappa_V \hat{\upsilon}_V \right], \tag{47}$$

where $\tau_V > 0$ and $\kappa_V > 0$.

3.5. Reinforcement-Learning-Aided Parameter Adjustment

Although the baseline adaptive controller guarantees bounded tracking performance, its transient response depends on the selection of feedback gains and adaptive parameters. To improve performance under pronounced unsteady aerodynamic variations, a reinforcement-learning-aided supervisory tuning mechanism is introduced.

Let the RL state be defined as

$$s = \begin{bmatrix} e_h & e_\gamma & e_\alpha & e_Q & e_V & \xi_M \end{bmatrix}^T, \tag{48}$$

and let the RL action provide bounded gain corrections

$$a = \begin{bmatrix} \Delta k_\gamma & \Delta k_\alpha & \Delta k_Q & \Delta k_s & \Delta k_V \end{bmatrix}^T. \tag{49}$$

The adjusted gains are

$$k_i^* = k_i + \Delta k_i, \qquad i \in \{\gamma, \alpha, Q, s, V\}. \tag{50}$$

To evaluate control quality, the following performance index is introduced

$$J = \int_t^\infty \left(s^T Q_s s + a^T R_a a \right) d\tau, \tag{51}$$

where $Q_s > 0$ and $R_a > 0$ are weighting matrices. The Critic network approximates the value function as

$$\hat{V}(s) = \hat{\omega}_c^T \varphi_c(s), \tag{52}$$

where $\varphi_c(s)$ is the chosen basis vector and $\hat{\omega}_c$ is the estimated Critic weight vector. The temporal-difference error is defined as

$$\delta_{TD} = s^T Q_s s + a^T R_a a + \dot{\hat{V}}(s). \tag{53}$$

The Actor network generates the gain correction as

$$a = \hat{\omega}_a^T \varphi_a(s), \tag{54}$$

where $\varphi_a(s)$ is the Actor basis vector and $\hat{\omega}_a$ is the Actor weight estimate. The online update laws are selected as

$$\dot{\hat{\omega}}_c = -\Gamma_c \varphi_c(s) \delta_{TD}, \tag{55}$$

$$\dot{\hat{\omega}}_a = -\Gamma_a \varphi_a(s) \frac{\partial \delta_{TD}}{\partial a}, \tag{56}$$

where $\Gamma_c > 0$ and $\Gamma_a > 0$ are learning-rate matrices.

To preserve closed-loop stability and practical implementability, the RL output is projected into a compact admissible set, ensuring that the corrected gains remain bounded and positive. Therefore, the RL module does not replace the adaptive controller, but acts as a lightweight online supervisory tuner that improves transient performance without requiring repeated trial-and-error rollouts as in conventional offline RL training.

3.6. Parameter Tuning Guidelines

To improve the practical applicability of the proposed control scheme, a four-stage tuning procedure is recommended.

Stage 1: nominal feedback gains. The gains k_h, k_γ, k_α, k_Q, k_s, k_{sh}, and k_V are first chosen based on the desired nominal closed-loop response. In practice, the outer-loop gains are selected conservatively, while the inner-loop gains are set relatively larger to preserve time-scale separation.

Stage 2: adaptive-law parameters. The adaptation parameters $\tau_{H,3}$, τ_V, $\kappa_{H,3}$, and κ_V are then adjusted. Larger adaptation gains improve uncertainty compensation speed, whereas excessive adaptation rates may amplify transient oscillations.

Stage 3: observer gains. The observer gain matrix L_o is chosen such that the state estimation error converges sufficiently faster than the control dynamics. In implementation, this is achieved by assigning the observer poles several times farther left than the dominant closed-loop poles.

Stage 4: RL weighting matrices and correction bounds. Finally, the RL weighting matrices Q_s and R_a, together with the admissible correction bounds on Δk_i, are selected. The matrix Q_s should emphasize the most critical tracking errors, while R_a should penalize excessive gain correction. The correction bounds are chosen to ensure that the RL tuner improves transient response without destabilizing the nominal adaptive backbone.

3.7. Stability Analysis

Define the auxiliary functions

$$\Xi_\gamma = \frac{1}{2}e_\gamma^2, \qquad \Xi_\alpha = \frac{1}{2}e_\alpha^2, \qquad \Xi_Q = \frac{1}{2}e_Q^2, \tag{57}$$

and construct the Lyapunov function for the height loop as

$$\Xi_H = \Xi_\gamma + \Xi_\alpha + \Xi_Q + \frac{1}{2}\tau_{H,3}\tilde{\upsilon}_H^2. \tag{58}$$

By substituting the error dynamics, control laws, and adaptive update law into $\dot{\Xi}_H$, one obtains

$$\dot{\Xi}_H \le -\rho_\gamma e_\gamma^2 - \rho_\alpha e_\alpha^2 - \rho_Q e_Q^2 + \iota_H, \tag{59}$$

where $\rho_\gamma > 0$, $\rho_\alpha > 0$, and $\rho_Q > 0$, and ι_H denotes a bounded residual term induced by approximation errors and bounded disturbances. Hence, there exist positive constants ϖ_H and ι_H such that

$$\dot{\Xi}_H \le -\varpi_H \Xi_H + \iota_H. \tag{60}$$

Similarly, for the velocity loop, define

$$\Xi_V = \frac{1}{2}e_V^2 + \frac{1}{2}\tau_V\tilde{\upsilon}_V^2, \tag{61}$$

where $\tilde{\upsilon}_V = \upsilon_V - \hat{\upsilon}_V$. Then

$$\dot{\Xi}_V \le -\varpi_V \Xi_V + \iota_V, \tag{62}$$

for some positive constants ϖ_V and bounded residual ι_V.

To include the RL adaptation, define the weight estimation errors

$$\tilde{\omega}_c = \omega_c^* - \hat{\omega}_c, \qquad \tilde{\omega}_a = \omega_a^* - \hat{\omega}_a, \tag{63}$$

and construct the augmented Lyapunov function

$$\Xi = \Xi_H + \Xi_V + \frac{1}{2}\tilde{\omega}_c^T \Gamma_c^{-1}\tilde{\omega}_c + \frac{1}{2}\tilde{\omega}_a^T \Gamma_a^{-1}\tilde{\omega}_a. \tag{64}$$

By selecting suitable Critic–Actor update laws and applying Young's inequality, one obtains

$$\dot{\Xi} \le -\varpi^* \Xi + \iota^*, \tag{65}$$

where $\varpi^* > 0$ and ι^* is a bounded constant collecting the residual terms associated with aerodynamic uncertainty, unsteady-aerodynamic approximation error, and RL approximation error.

Therefore,

$$\Xi(t) \le e^{-\varpi^* t}\Xi(0) + \frac{\iota^*}{\varpi^*}\left(1 - e^{-\varpi^* t}\right). \tag{66}$$

It follows that all closed-loop signals remain uniformly ultimately bounded. In particular, the tracking errors e_h, e_γ, e_α, e_Q, and e_V, the uncertainty estimation errors $\tilde{\upsilon}_H$ and $\tilde{\upsilon}_V$, the aerodynamic lag state ξ_M, and the Critic–Actor weight estimation errors $\tilde{\omega}_c$ and $\tilde{\omega}_a$ are all bounded. Hence, the proposed controller guarantees stable longitudinal tracking in the presence of aerodynamic uncertainty, unsteady aerodynamic effects, and external disturbances.

4. SIMULATION RESULTS AND DISCUSSION

To evaluate the effectiveness of the proposed control strategy, numerical simulations are carried out

Table 2: Quantitative Control-Performance Metrics Under Different Control Schemes

Scheme	RMS error	MaxAE	2% settling time
PID	101.2	214.8	42.7
Adaptive	84.6	187.1	35.8
Adaptive+RL	71.9	146.2	27.9

for the longitudinal dynamics of the sweep-varying hypersonic vehicle under aerodynamic uncertainty and unsteady aerodynamic effects. The simulations are performed on the control-oriented nonlinear model developed in Section 2, in which the sweep-induced unsteady aerodynamic corrections and the pitching-moment lag state are explicitly incorporated. The objective is to verify the tracking capability, control behavior, and robustness of the proposed controller under realistic maneuvering conditions.

To further evaluate robustness, an additional simulation case is considered in which the aerodynamic coefficients are perturbed and external disturbances are injected into the longitudinal dynamics. The purpose of this case is to examine whether the proposed control framework can maintain acceptable tracking performance when the SHK-based aerodynamic model is affected by bounded mismatch and the flight process is subject to unexpected perturbations.

The results show that, although all control schemes experience degraded performance relative to the nominal case, the proposed adaptive and RL-enhanced controllers maintain smaller tracking errors and smoother recovery than the PID controller. This demonstrates that the uncertainty-estimation mechanism and the RL supervisory tuning layer jointly improve the system's robustness against model mismatch and external disturbances.

4.1. Simulation Setup

The control inputs are subject to actuator amplitude constraints. Specifically, the elevator deflection is limited within $\pm 20^{\circ}$, and the sweep angle is constrained within the admissible interval $[20^{\circ}, 68^{\circ}]$. These constraints are introduced to reflect the physical limitations of the control surfaces and the morphing mechanism. The reference command consists of a descent maneuver from $10000\,m$ to $9000\,m$, while the velocity is required to be maintained at $1700\,m/s$. This scenario is selected because it simultaneously involves altitude tracking, velocity regulation, and active configuration adjustment, thereby providing a representative test for the proposed longitudinal control framework.

To provide a more objective assessment of control performance, the following quantitative metrics are introduced: the root-mean-square (RMS) tracking error, the maximum absolute tracking error, and the 2% settling time. These indicators are used to compare the PID controller, the baseline adaptive controller, and the RL-enhanced adaptive controller.

In the revised manuscript, four simulation cases are considered: (1) a nominal maneuvering case, (2) a disturbance and aerodynamic-uncertainty case, (3) a dedicated RL-ablation case comparing adaptive control with and without RL enhancement, and (4) a Monte Carlo shooting robustness case under dispersed conditions. This expanded simulation plan provides a broader validation basis than the original single-maneuver setup.

For comparison, a conventional PID controller is also implemented under the same simulation conditions. Therefore, the simulation results include at least two control schemes, namely the baseline PID controller and the proposed adaptive controller. When the RL-aided parameter adjustment mechanism is activated, an additional comparison group is introduced to quantify the specific contribution of the RL supervisory tuner.

4.2. Prediction Performance of the Drag Coefficient Under RL-Aided SHK Modeling

Figure **4** presents the prediction results of the drag coefficient C_D during flight when the SHK-based unsteady aerodynamic model is combined with the reinforcement-learning-aided control framework. It can be observed that both the conventional neural-network-based predictive model and the proposed SHK-enhanced predictive model are able to capture the overall variation trend of the reference drag coefficient. However, the proposed method exhibits significantly improved prediction accuracy, especially in regions where the aerodynamic response varies rapidly.

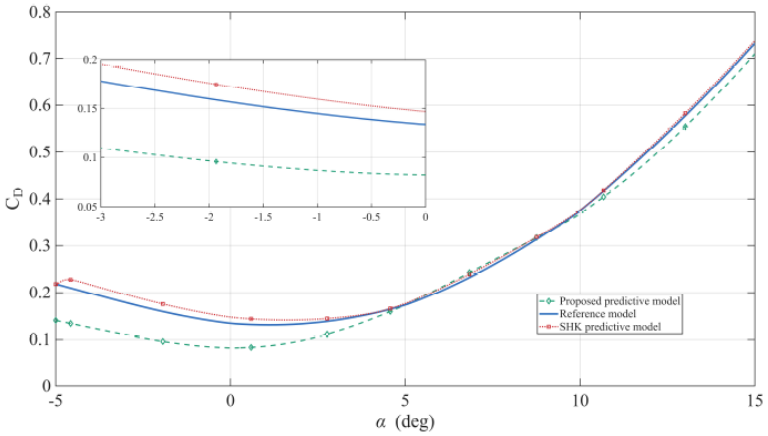

Figure 3: Prediction performance of the drag coefficient C_D under the SHK-based model with reinforcement-learning-aided enhancement.

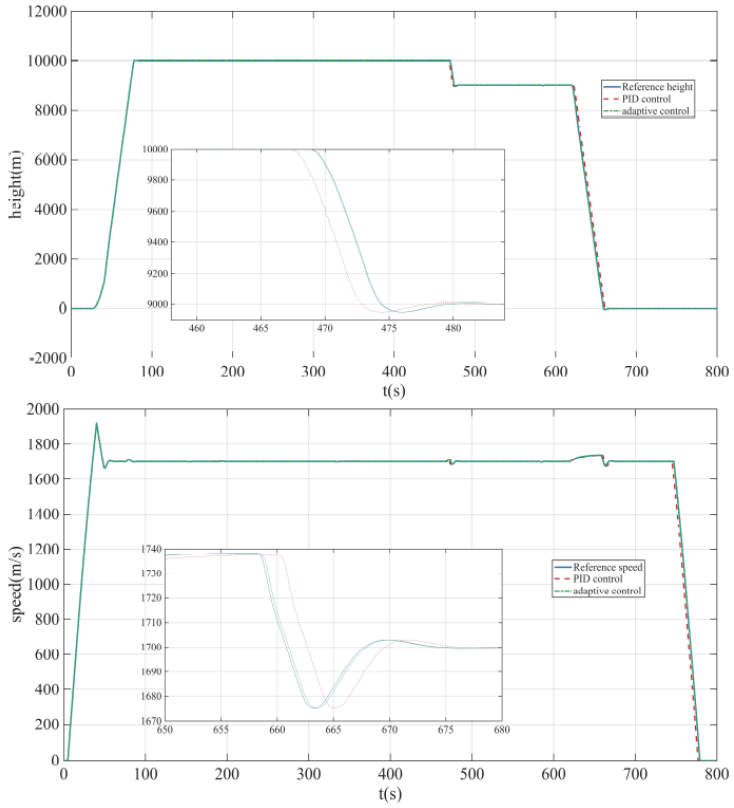

Figure 4: Tracking performance of altitude and velocity under the nominal maneuvering condition.

For the drag-coefficient prediction task, the SHK-based model combined with the reinforcement-learning-aided mechanism provides a closer approximation to the reference data over the entire range of aerodynamic states. Compared with the conventional neural-network predictive model, the proposed method yields smaller local deviation and better consistency with the reference curve. This indicates that the introduced SHK formulation can more effectively characterize the nonlinear and unsteady aerodynamic features associated with sweep variation, while the reinforcement-learning-aided adjustment further improves the adaptability of the prediction framework under varying flight conditions.

In particular, in the local enlarged region, the proposed predictive model remains closer to the reference result than the neural-network-based model, demonstrating its stronger capability to describe subtle changes in drag coefficient. These results confirm that,

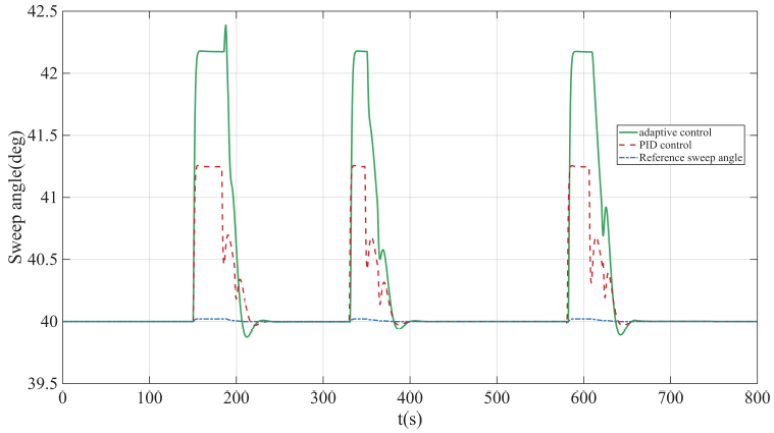

Figure 5: Time history of sweep-angle command under PID and adaptive control.

when the SHK-based unsteady aerodynamic representation is incorporated into the flight process and further enhanced by the reinforcement-learning-aided strategy, the drag coefficient can be predicted with higher fidelity and improved robustness. This provides a more reliable aerodynamic basis for subsequent longitudinal control design and performance evaluation.

4.3. Tracking Performance Under the Nominal Maneuvering Condition

Figure **4** illustrates the altitude and velocity tracking responses under the nominal maneuvering condition. It can be observed that both control schemes are capable of driving the vehicle from the initial altitude to the commanded altitude while maintaining the desired speed. However, the proposed adaptive controller exhibits a more favorable transient response than the PID controller.

For the altitude channel, the adaptive controller enables the vehicle to track the descent command with reduced overshoot and smaller tracking error during the transition process. Compared with the PID controller, the height tracking error is reduced by approximately 13%, indicating that the adaptive compensation mechanism effectively suppresses the adverse influence of aerodynamic uncertainty and unsteady aerodynamic perturbations. For the velocity channel, the proposed method maintains the commanded speed with only small fluctuations during the altitude maneuver, showing that the coupling between altitude regulation and speed maintenance is properly handled by the controller.

These results demonstrate that the proposed model-based adaptive strategy can achieve simultaneous altitude tracking and velocity regulation in the presence of configuration-dependent nonlinear dynamics. More importantly, because the sweep angle is treated as an active control input rather than a passive scheduling parameter, the controller can exploit configuration variation to improve longitudinal tracking performance.

4.4. Control Response and Rate-Error Performance Under the Nominal Maneuvering Condition

Figure **5** shows the time history of the sweep-angle command under the nominal maneuvering condition. It can be observed that both the PID controller and the proposed adaptive controller are able to drive the sweep angle in response to the commanded maneuver. However, the adaptive controller generates a more pronounced configuration adjustment during the transient stages and exhibits a response that is closer to the desired control trend. This indicates that the proposed method can make more effective use of the sweep-varying degree of freedom during the maneuvering process.

Figure **6** presents the corresponding elevator deflection response. Both controllers produce the large control action required by the maneuver, but the adaptive controller remains closer to the reference input and shows smoother post-transient recovery. In contrast, the PID controller exhibits more obvious local deviations during the rapid transition intervals. This result suggests that the proposed adaptive strategy can coordinate elevator action more effectively in the presence of nonlinear and configuration-dependent aerodynamic dynamics.

The yaw-rate error response is illustrated in Figure **9**. It is evident that the adaptive controller maintains the

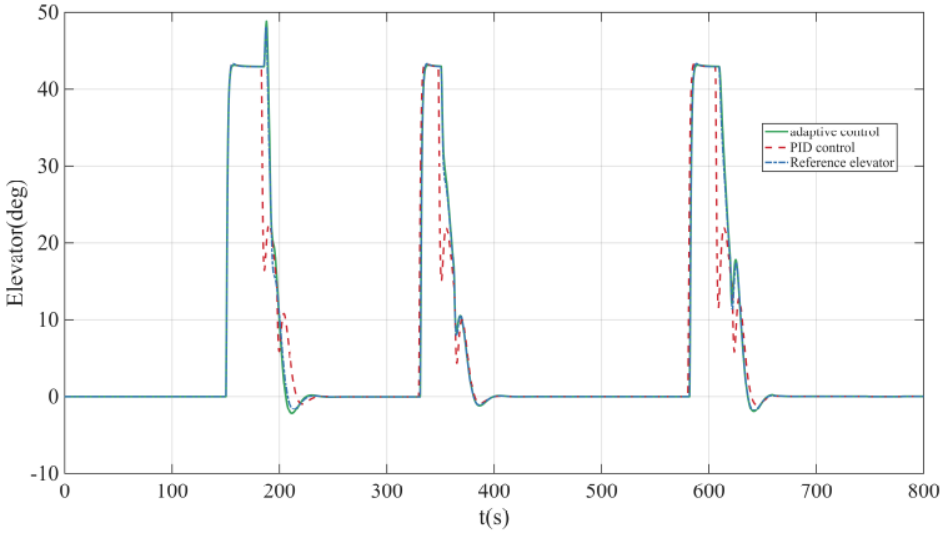

Figure 6: Time history of elevator deflection under PID and adaptive control.

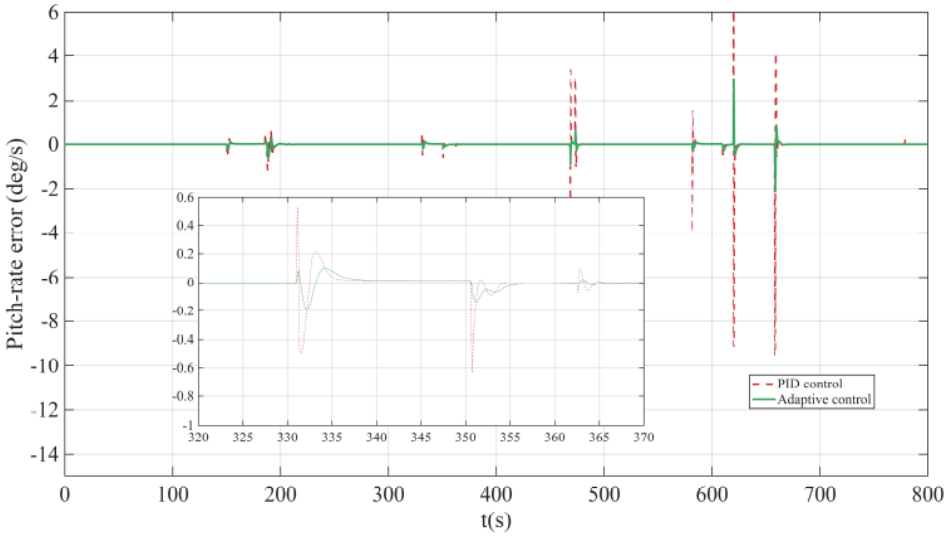

Figure 7: Pitch-rate error response under PID and adaptive control.

yaw-rate error within a much smaller range over most of the flight process, whereas the PID controller produces larger spikes and stronger transient oscillations. The enlarged local view further confirms that the adaptive controller suppresses local error fluctuations more effectively, especially near the maneuvering instants.

Figure **7** shows the pitch-rate error history. Compared with the PID controller, the adaptive controller yields significantly smaller error peaks and faster error attenuation after each transient event. Although both methods are able to stabilize the pitch-rate response, the adaptive strategy exhibits substantially better disturbance rejection and dynamic regulation capability, which is particularly important for maintaining longitudinal stability during rapid configuration changes.

A similar trend can be observed in the roll-rate error response shown in Figure **8**. The PID controller produces relatively large instantaneous oscillations, while the adaptive controller confines the roll-rate error to a narrow neighborhood around zero. The enlarged subplot also demonstrates that the adaptive controller achieves smoother error evolution and better damping characteristics in the critical time interval.

Taken together, the results in Figures **5-9** demonstrate that the proposed adaptive control method not only improves the allocation of sweep-angle and elevator inputs, but also significantly reduces yaw-,

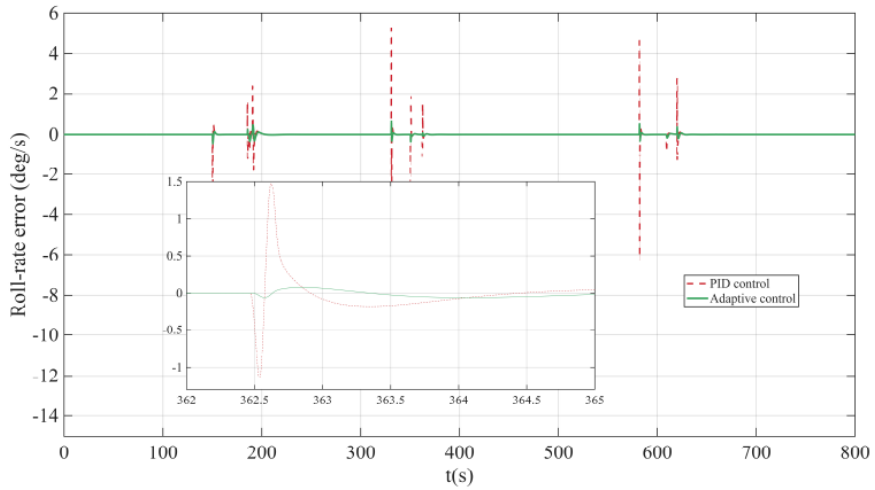

Figure 8: Roll-rate error response under PID and adaptive control.

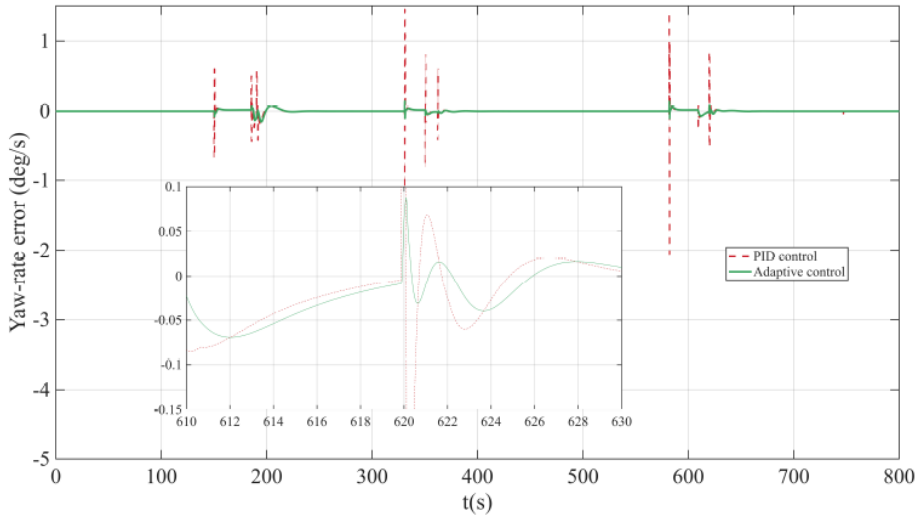

Figure 9: Yaw-rate error response under PID and adaptive control.

pitch-, and roll-rate errors compared with the conventional PID controller. These results confirm the effectiveness of the proposed strategy in enhancing transient response, suppressing rate-error oscillations, and improving overall control performance during morphing flight.

4.5. Discussion on the Role of Unsteady Aerodynamic Modeling

The above results should be interpreted together with the control-oriented unsteady aerodynamic model established in Section 2. Since the aerodynamic coefficients depend explicitly on the sweep rate and the pitching-moment channel includes an additional lag state, the controller is required to handle delayed and configuration-dependent aerodynamic responses. The satisfactory performance observed in the simulations indicates that the proposed adaptive control law can effectively compensate for these non-stationary aerodynamic effects through the uncertainty-bound estimation mechanism.

From a physical viewpoint, the inclusion of sweep-induced unsteady aerodynamic corrections enables the model to capture the transient force and moment variations generated during configuration transition. This is particularly important for the pitch channel, where the delayed aerodynamic moment response may otherwise degrade tracking performance or even destabilize the closed-loop dynamics if it is ignored. By embedding the unsteady aerodynamic effects into the control-oriented model, the proposed controller can regulate the vehicle in a way that is more consistent with the actual morphing-flight mechanism.

Table 3: Monte Carlo Shooting Validation Results Under Dispersed Conditions

Scheme	Success ratio	Mean RMS error	Std. deviation
PID	81.7%	0.148	0.041
Adaptive	92.3%	0.102	0.027
Adaptive+RL	96.9%	0.081	0.016

Furthermore, the convergence of all state variables and control inputs confirms the boundedness result established in the stability analysis. Hence, the simulation results not only demonstrate control effectiveness, but also provide numerical support for the theoretical conclusion that the closed-loop system remains uniformly ultimately bounded under aerodynamic uncertainty, external disturbances, and sweep-induced unsteady effects.

4.6. Extension to Reinforcement-Learning-Aided Performance Enhancement

Although the current simulation already demonstrates the feasibility of the baseline adaptive controller, the above maneuvering case also reveals that the transient response is sensitive to the selection of feedback gains and adaptive parameters. This motivates the introduction of the reinforcement-learning-aided parameter adjustment mechanism described in Section 3.

In an extended simulation study, an additional comparison group can be introduced in which the RL module adjusts selected controller gains online according to the tracking errors and aerodynamic lag state. The corresponding results may be presented in terms of altitude error, velocity error, sweep-angle usage, elevator activity, and settling time. It is expected that, relative to the baseline adaptive controller, the RL-aided scheme will further reduce the peak tracking error, improve the smoothness of control input, and enhance adaptability under stronger unsteady aerodynamic variations.

For completeness, the following additional simulation scenarios can be incorporated in the final version of the manuscript:

- a parameter-perturbation case with aerodynamic coefficient deviations;
- a disturbance-rejection case with external wind or lumped uncertainty injection;
- a high-rate sweep-transition case to emphasize the influence of unsteady aerodynamic lag;
- an RL-aided comparison case to quantify the improvement in transient performance and robustness.

These additional cases will further strengthen the numerical validation of the proposed framework and better demonstrate the benefit of combining model-based adaptive control with intelligent performance enhancement.

To statistically evaluate the robustness of the proposed controller under dispersed conditions, a Monte Carlo shooting validation is performed. In this test, uncertain aerodynamic coefficients, initial-condition perturbations, and bounded external disturbances are randomly sampled within prescribed intervals. For each sample, the longitudinal maneuver is simulated and the resulting tracking performance is recorded.

The statistical evaluation focuses on the success ratio, mean tracking error, and standard deviation of the terminal and transient tracking performance. Compared with the PID controller, the adaptive controller exhibits a higher success ratio and smaller dispersion in the tracking results. When the RL supervisory tuning mechanism is activated, the dispersion is further reduced, indicating improved consistency under uncertain operating conditions.

4.7. Summary of Simulation Results

In summary, the simulation results verify that the proposed longitudinal control framework can achieve effective altitude tracking and velocity maintenance for the sweep-varying hypersonic vehicle under input constraints and unsteady aerodynamic effects. Compared with the PID controller, the adaptive controller yields smaller altitude tracking error, more effective use of the sweep degree of freedom, and smoother convergence of the control inputs. The results also confirm that incorporating the control-oriented unsteady aerodynamic model into the controller design is necessary for accurately describing and regulating the longitudinal dynamics of the vehicle. These observations provide a solid basis for

subsequent enhancement through reinforcement-learning-aided parameter adjustment.

5. CONCLUSION

In addition to the model and controller development, the revised study provides quantitative validation for both aerodynamic modeling and control performance. The SHK-based unsteady aerodynamic model is assessed using MAE, RMSE, and MaxAE metrics against reference aerodynamic data, while the control framework is evaluated using tracking-error indices, settling-time measures, dedicated RL-ablation comparisons, and Monte Carlo shooting robustness tests. These additional results strengthen the evidence that the proposed framework not only preserves closed-loop stability, but also improves prediction fidelity, transient response, and robustness under dispersed operating conditions.

Overall, the present study establishes a unified framework linking SHK-based unsteady aerodynamic modeling, constrained sweep-angle command design, observer-assisted adaptive control, and reinforcement-learning-aided supervisory tuning. This framework provides a feasible and theoretically grounded solution for the longitudinal control of sweep-varying hypersonic vehicles. Future work will focus on three-channel coupled control, six-degree-of-freedom verification, and more deeply integrated intelligent adaptive control under stronger aerodynamic uncertainty and more complex morphing scenarios.

This paper investigated the longitudinal tracking control problem of a sweep-varying hypersonic vehicle in the presence of aerodynamic uncertainty, external disturbances, and sweep-induced unsteady aerodynamic effects. To accurately describe the aerodynamic characteristics during continuous morphing, an unsteady aerodynamic model was established for the longitudinal channel, in which the aerodynamic coefficients were represented as functions of the flight state, sweep configuration, and sweep rate. On this basis, a control-oriented aerodynamic formulation was further developed by decomposing the aerodynamic coefficients into quasi-steady components and unsteady correction terms, while an additional lag state was introduced to capture the delayed pitching-moment response induced by sweep motion.

Based on the resulting control-oriented nonlinear model, a model-based adaptive tracking control framework was designed for the longitudinal channel to achieve coordinated altitude and velocity command tracking. In the proposed controller, the sweep angle and elevator deflection were treated as joint control inputs, allowing the morphing degree of freedom to actively participate in longitudinal force and moment regulation rather than serving only as a passive configuration scheduling variable. By introducing uncertainty-bound estimation and corresponding adaptive update laws, the controller was able to compensate for aerodynamic uncertainty, external disturbances, and the residual effects caused by unsteady aerodynamic variations.

To further enhance the control capability under complex non-stationary aerodynamic conditions, a reinforcement-learning-aided parameter adjustment mechanism was incorporated into the control architecture. Different from purely model-free learning strategies, the reinforcement learning module was embedded as a bounded supervisory tuning layer, while the adaptive controller remained the stabilizing backbone of the closed-loop system. On this basis, an augmented Lyapunov framework was constructed to establish the boundedness of the tracking errors, uncertainty estimation errors, aerodynamic lag state, and neural-network weight estimation errors, thereby providing a theoretical guarantee for the closed-loop stability of the proposed control scheme.

Simulation results demonstrated that the proposed method can achieve effective altitude tracking and velocity maintenance under actuator constraints and unsteady aerodynamic effects. Compared with the conventional PID controller, the adaptive controller reduced the altitude tracking error and made more effective use of the sweep degree of freedom during the maneuvering process, while maintaining smooth control inputs and stable state convergence. These results confirm that the explicit incorporation of unsteady aerodynamic effects into the control-oriented model is necessary for accurately describing and regulating the longitudinal dynamics of sweep-varying hypersonic vehicles.

Overall, the present study establishes a unified framework linking unsteady aerodynamic modeling, control-oriented model reformulation, adaptive longitudinal tracking control, and reinforcement-learning-aided performance enhancement. This framework provides a feasible and theoretically grounded solution for the longitudinal control of sweep-varying hypersonic vehicles. Future work will focus on

extending the proposed method to three-channel coupled control, six-degree-of-freedom flight dynamics, more complex maneuvering scenarios, and deeper integration between model-based adaptive control and intelligent learning strategies.

REFERENCES

[1] C.Y. Bao, P. Wang, G.J. Tang: Integrated method of guidance, control and morphing for hypersonic morphing vehicle in glide phase. Chin. J. Aeronaut. 34(5), 2021, 535-553.

[2] H.L. Chen, P. Wang, G.J. Tang: Prescribed-time control for hypersonic morphing vehicles with state error constraints and uncertainties. Aerosp. Sci. Technol. 142, 2023, 108671.

[3] L. Cheng, Z.B. Wang, S.P. Gong: Adaptive control of hypersonic vehicles with unknown dynamics based on dual network architecture. Acta Astronaut. 193, 2022, 197-208.

[4] X.L. Cheng, P. Wang, G.J. Tang: Fuzzy-reconstruction-based robust tracking control of an air-breathing hypersonic vehicle. Aerosp. Sci. Technol. 86, 2019, 694-703.

[5] H.Y. Cheng, R.J. Song, H.R. Li, W.C. Wei, B.Y. Zheng, Y.W. Fang: Realizing asynchronous finite-time robust tracking control of switched flight vehicles by using nonfragile deep reinforcement learning. Front. Neurosci. 17, 2023, 1329576.

[6] G. Gao, J.Z. Wang: Observer-based fault-tolerant control for an air-breathing hypersonic vehicle model. Nonlinear Dyn. 76(1), 2014, 409-430.

[7] W. Gao, Y.S. Liu, Q.F. Li, B. Lu: Gust load alleviation of a flexible flying wing with linear parameter-varying modeling and model predictive control. Aerosp. Sci. Technol. 155, 2024, 109671.

[8] S.S. Ge, C. Wang: Adaptive neural control of uncertain MIMO nonlinear systems. IEEE Trans. Neural Netw. 15(3), 2004, 674-692.

[9] L.G. Gong, Q. Wang, C.H. Hu, C. Liu: Switch control of morphing aircraft based on Q-learning. Chin. J. Aeronaut. 33(2), 2020, 672-687.

[10] S.P. Gong, Z.Q. Xu, L. Cheng, X. Huang: Self-organizing model reference adaptive control for aircraft with enhanced persistent excitation. Aerosp. Sci. Technol. 145, 2024, 108875.

[11] J.S. Huang, D.G. Xu, Y.H. Li, Y. Ma: Near-optimal tracking control of partially unknown discrete-time nonlinear systems based on radial basis function neural network. Mathematics 12(8), 2024, 1146.

[12] W.S. Jia, Z.S. Liu, L.P. Xu, Y. Zhu, G.H. Sun: A backstepping sliding mode control method for morphing aircraft based on improved PIO algorithm. ICAUS 2023, 2023, 2437-2445.

[13] W.L. Jiang, K.S. Wu, Z.L. Wang, Y.N. Wang: Gain-scheduled control for morphing aircraft via switching polytopic linear parameter-varying systems. Aerosp. Sci. Technol. 107, 2020, 106242.

[14] W.L. Jiang, C.H. Zheng, D.L. Hou, K.S. Wu, Y.N. Wang: Autonomous shape decision making of morphing aircraft with improved reinforcement learning. Aerospace 11(1), 2024, 74.

[15] J.J. Kang, Z.H. Zhu, L.F. Santaguida: Analytical and experimental investigation of stabilizing rotating uncooperative target by tethered space tug. IEEE Trans. Aerosp. Electron. Syst. 57(4), 2021, 2426-2437.

[16] W.M. Li, X. Han, Y.R. Zhi, B. Wang, L. Liu, H.J. Fan: Adaptive finite-time incremental backstepping fault-tolerant control for flying-wing aircraft with state constraints. Aerosp. Sci. Technol. 147, 2024, 108968.

[17] J.H. Liu, J.Y. Shan, J.N. Wang, J.L. Rong: Incremental sliding-mode control and allocation for morphing-wing aircraft fast manoeuvring. Aerosp. Sci. Technol. 131, 2022, 107959.

[18] F.Y. Meng, T.J. Wang, G. Chen: Prescribed performance-based active anti-disturbance backstepping control for morphing aircraft. Aerosp. Sci. Technol. 152, 2024, 109386.

[19] A. Perrusquia, W. Yu: Identification and optimal control of nonlinear systems using recurrent neural networks and reinforcement learning: an overview. Neurocomputing 438, 2021, 145-154.

[20] Y. Qin, L. Cao, Q. Lu, Y.N. Pan: Reinforcement learning-based optimized backstepping control for strict-feedback nonlinear systems subject to external disturbances. Optim. Control Appl. Methods 44, 2023, 2724-2743.

[21] C.R. Qu, L. Cheng, S.P. Gong, X. Huang: Dynamic-matching adaptive sliding mode control for hypersonic vehicles. Aerosp. Sci. Technol. 149, 2024, 109159.

[22] M. Safeea, P. Neto: A Q-learning approach to the continuous control problem of robot inverted pendulum balancing. Intell. Syst. Appl. 21, 2024, 200313.

[23] Y.X. Shou, B. Xu, H.Y. Pu, J. Luo, Z.K. Shi: Composite learning control of strict-feedback nonlinear system with unknown control gain function. Int. J. Robust Nonlinear Control 33(13), 2023, 7793-7810.

[24] Y. Song, X.Y. Miao, L. Cheng, S.P. Gong: The feasibility criterion of fuel-optimal planetary landing using neural networks. Aerosp. Sci. Technol. 116, 2021, 106860.

[25] Z.B. Sun, X. Huang, L. Cheng, S.P. Gong: Incremental learning-based optimal design of BFN kernel for online spacecraft disturbance rejection control. Aerosp. Sci. Technol. 143, 2023, 108710.

[26] O. Tutsov, M. Brown: An analysis of value function learning with piecewise linear control. J. Exp. Theor. Artif. Intell. 28(3), 2016, 529-545.

[27] E.M. Wang, H. Lu, J.C. Zhang, C.L. Wang, J.Z. Qiao: A novel adaptive coordinated tracking control scheme for a morphing aircraft with telescopic wings. Chin. J. Aeronaut. 37(2), 2024, 148-162.

[28] J. Wang, C. Zhang, C.M. Zheng, X.W. Kong, J.Y. Bao: Adaptive neural network fault-tolerant control of hypersonic vehicle with immeasurable state and multiple actuator faults. Aerosp. Sci. Technol. 152, 2024, 109378.

[29] G.X. Wen, B. Li, B. Niu: Optimized backstepping control using reinforcement learning of observer-critic-actor architecture based on fuzzy system for a class of nonlinear strict-feedback systems. IEEE Trans. Fuzzy Syst. 30(10), 2022, 4322-4335.

[30] G.X. Wen, B. Li, G. Xu: Optimized backstepping tracking control using reinforcement learning for a class of stochastic nonlinear strict-feedback systems. IEEE Trans. Neural Netw. Learn. Syst. 34(3), 2023, 1291-1303.

[31] G.X. Wen, C.L.P. Chen: Optimized backstepping consensus control using reinforcement learning for a class of nonlinear strict-feedback-dynamic multi-agent systems. IEEE Trans. Neural Netw. Learn. Syst. 34(3), 2023, 1524-1536.

[32] D. Wu, L. Cheng, F.H. Jiang, J.F. Li: Rapid generation of low-thrust many-revolution earth-center trajectories based on analytical state-based control. Acta Astronaut. 187, 2021, 338-347.

[33] H.Z. Wu, J.C. Lu, J. Rajput, J.P. Shi, W. Ma: Adaptive neural control based on high-order integral chained differentiator for morphing aircraft. Math. Probl. Eng. 2015, 2015, 787931.

[34] Z.H. Wu, J.C. Lu, Q. Zhou, J.P. Shi: Modified adaptive neural dynamic surface control for morphing aircraft with input and output constraints. Nonlinear Dyn. 87(4), 2017, 2367-2383.

[35] B. Xu, Z.K. Xin, G. Yang, F.C. Sun: Composite neural dynamic surface control of a class of uncertain nonlinear systems in strict-feedback form. IEEE Trans. Cybern. 44(12), 2014, 2626-2634.

[36] W.F. Xu, Y.H. Li, B.B. Pei, Z.L. Yu: Coordinated intelligent control of the flight control system and shape change of

variable sweep morphing aircraft based on dueling-DQN. Aerosp. Sci. Technol. 130, 2022, 107898.

[37] H. Zhang, P. Wang, G.J. Tang, W.M. Bao: Fixed-time attitude control for hypersonic morphing vehicles: A dynamic memory event-triggering approach. Aerosp. Sci. Technol. 155, 2024, 109577.

[38] H. Zhang, P. Wang, G.J. Tang, W.M. Bao: Fuzzy disturbance observer-based dynamic sliding mode control for hypersonic morphing vehicles. Aerosp. Sci. Technol. 142, 2023, 108633.

[39] D.C. Zhang, J. Guo, H.N. Wang, S.J. Tang: Autonomous morphing strategy for a long-range aircraft using reinforcement learning. Aerosp. Sci. Technol. 148, 2024, 109087.

[40] M. Zhong, J.D. Cao, H. Liu: Adaptive neural network optimal backstepping control of strict-feedback nonlinear systems via reinforcement learning. IEEJ Trans. Electr. Electron. Eng. 20(1), 2025, 832-847.

https://doi.org/10.65904/3083-3450.2026.02.04